Theoretical analysis and experiment on gas film stiffness with slip flow in a spiral-grooved dry gas seal

Junjie Lu
College of Mechanical and Electrical and Energy Engineering, NingboTech University, Ningbo, China

Abstract

Purpose – This study aims to study the gas film stiffness of the spiral groove dry gas seal.

Design/methodology/approach – The present study represents the first attempt to calculate gas film stiffness in consideration of the slipping effect by using the new test technology for dry gas seals. First, a theoretical model of modified generalized Reynolds equation is derived with slipping effect of a micro gap for spiral groove gas seal. Second, the test technology examines micro-scale gas film vibration and stationary ring vibration to determine gas film stiffness by establishing a dynamic test system.

Findings – An optimum value of the spiral angle and groove depth for improved gas film stiffness is clearly seen: the spiral angle is 1.34 rad (76.8°) and the groove depth is 1×10^{-5} m. Moreover, it can be observed that optimal structural parameters can obtain higher gas film stiffness in the experiment. The average error between experiment and theory is less than 20%.

Originality/value – The present study represents the first attempt to calculate gas film stiffness in consideration of the slipping effect by using the new test technology for dry gas seals.

Keywords Optimization, Stiffness, Test, Gas seal, Structure parameters

Paper type Research paper

Nomenclature and units

A_e = effective area of static ring, m^2;
E = half of groove depth, m;
$2E$ = groove depth, m;
F_o = opening force, N;
F_c = closing force, N;
F_s = spring force, N;
H = non-dimensional lubrication film thickness;
h = lubrication film thickness, m;
K_g = theoretical gas film stiffness, N/m;
K'_g = experimental gas film stiffness, N/m;
k_n = Knudsen number;
K_s = spring stiffness, N/mm;
l = molecular free path, m;
n = groove number;
n_r = rotational speed, rad/s;
n_s = spring number;
P = non-dimensional gas film pressure;
p = pressure of gas film, Pa;
p_i = inlet pressure, Pa;
p_o = outlet pressure, Pa;
R_i = inner radius, m;
R_o = outer radius, m;
R_r = root radius, m;
R_e = slip radius, m;
r = seal ring radius, m;
U_0 = linear velocity of the inner radius of a seal ring, m/s;
u = circumferential velocity of gas film, m/s; and
v = radial velocity of gas film, m/s.

Greek symbols

α = complementary angle of spiral angle, rad;
β = spiral angle, rad;
β_0 = groove coefficient;
δ = gas film thickness, m;
ε = small parameter of iterative perturbation;
ζ = non-dimensional radius;
ζ_o = non-dimensional outer radius;
μ = dynamic viscosity of gas, Pa.s;
ρ = gas density, kg/m3;
σ_v = coefficient of the adjustment in the molecular tangential; momentum;
φ = non-dimensional angle;
χ = compressible correction coefficient under slip boundary condition;
ω = equivalent spiral angle;

The current issue and full text archive of this journal is available on Emerald Insight at: **https://www.emerald.com/insight/0036-8792.htm**

Industrial Lubrication and Tribology
73/10 (2021) 1226–1236
Emerald Publishing Limited [ISSN 0036-8792]
[DOI 10.1108/ILT-03-2021-0075]

Received 18 March 2021
Revised 6 June 2021
11 August 2021
Accepted 11 August 2021

Industrial Lubrication and Tribology
Volume 73 · Number 10 · 2021 · 1226–1236

Λ = compressible coefficient;
$\triangle_x$ = stationary ring axial vibration value; and
$\triangle_\delta$ = gas film axial vibration value.

Integration constant

A^i (i = 1, 2, 3);
B^i (i = 1, 2, 3);
c^{ij} (i = 1, 2 and j = 0, 1); and
c'^{ij} (i = 1, 2 and j = 0, 1).

1. Introduction

Because of the gas film thickness of the spiral groove dry gas seal is only 3–6 μm. The vibration, which is from a dry gas seal system, rotating equipment or external environment, leads to wear and abrasion of seal faces. The stability of the dry gas seal is broken. Thus, the performance of gas film stiffness plays a key role in the stability of dry gas seals (Ding and Lu, 2016).

In the previous study, Miller *et al.* used the step jump method and a novel direct numerical frequency response method to compute the gas film stiffness and damping properties of a spiral grooved mechanical face seal (Miller and Green, 2002, 2003). Sawicki *et al.* investigated the variation of nonlinear stiffness and damping coefficients in a journal orbit with respect to equilibrium position (Sawicki and Rao, 2004). Liu *et al.* studied the dynamic characteristics of bearing with spiral grooves (Liu *et al.*, 2012). The results showed the decrease in the stiffness become obvious with the increase of the compressibility number. Shi *et al.* developed a numerical model based on the Reynolds equation to investigate the load-carrying performance including gas film stiffness (Shi *et al.*, 2016). Xu *et al.* presented a new design of shroud seal by using spiral-grooved gas face seal theory and analyzing the stiffness (Xu and Yang, 2016). A novel hole-pattern damping seal with a special-shaped three-dimensional hole cavity was proposed to enhance leakage and rotordynamic performance (Zhang *et al.*, 2021). Ding *et al.* considered the heat dissipation of gas film and studied gas film stiffness under theory and experiment (Ding *et al.*, 2014). Jiang *et al.* introduced a series of bionic grooves based on bird wings (Jiang *et al.*, 2016). A theoretical model solved with finite difference method is developed to study the static sealing performance and gas film stiffness is 20% larger than of common spiral groove dry gas seal. Bai *et al.* developed a new mathematical model of the electro-viscosity based on the Poisson–Boltzmann equation (Bai *et al.*, 2006). The analysis results showed that the electro-viscosity leads to a significant increase in the lubricated film thickness. Shen *et al.* studied the optimal parameters of a dynamic vibration absorber with stiffness and a new strategy is presented to obtain the optimum negative stiffness ratio (Shen *et al.*, 2017). The performance of supercritical dry gas seal with a different deep spiral groove was investigated with the thermal-fluid-solid coupling method, the results showed that the average film pressure, open force and leakage decreased while the average face temperature and flow velocity increased as the spiral groove number increases (Du and Zhang, 2019). Kollinger *et al.* used an experiment to study the axial motivation vibration of a mechanical seal under a stable working condition (Kollinger, 1989). Kolozmoets *et al.* designed a test bench and tested gas-dynamic seal and obtained data variation of operating conditions, such as leakage and dynamic behavior (Kolomoets and Dotsenko, 2012). Huang *et al.* used acoustic emission testing to investigate the starting process and the stopping process of a double dry gas seal (Huang *et al.*, 2013; Huang *et al.*, 2013). The computational fluid dynamics and experiments are carried out by Yu to investigate the influence of perturbations on the dynamic stiffness of aerostatic bearings (Yu *et al.*, 2015). Jin *et al.* introduced a new type of analysis method to seek the actual working performance of the dry gas seal, meanwhile, the dry gas seal was manufactured to verify the theoretical analysis by measuring the inward leakage (Jin *et al.*, 2016). Jacobs *et al.* used the experimental method to investigate the formation of a lubricant film in a deep groove ball bearing and its effect on the dynamics (Jacobs *et al.*, 2014). Meanwhile, researchers have also developed intelligent numerical approaches to analyze the effects of groove shape (Nagai *et al.*, 2018; Kou *et al.*, 2020), groove pattern (Lu, 2020) and micro-sequence on the groove bottom (Lu *et al.*, 2021) on the sealing performances of the seal. These studies have demonstrated that the micro-gap between the sealing rings and the characteristics of the spiral groove profoundly influence gas flow through the seal.

However, there are some insufficiencies in gas film stiffness analysis of spiral groove dry gas seal:

- There is a lack of approximate theory to analyze the mechanism of gas film.
- The testing of the dynamic performance of dry gas seal lags, such as the displacement and vibration of the sealing ring, is little.

The present study represents the first attempt to calculate gas film stiffness in consideration of the slipping effect by using the new test technology for dry gas seals. First, a theoretical model of modified generalized Reynolds equation is derived with slipping effect of a micro gap for spiral groove gas seal. Approximate analytical expressions of opening force and stiffness of gas film is obtained by solving the non-linear Reynolds equation with the linear PH method and iterative method. Then, according to the changing trend of gas film stiffness, the optimization parameters of the spiral groove structure are discussed. Second, the test technology for gas film stiffness is difficult to implement in the dry gas sea because the clearance of the seal faces is only 3–6 μm. This work examines micro-scale gas film vibration and stationary ring vibration to determine gas film thickness and stiffness by establishing a dynamic test system for dry gas seals with LABVIEW, and then by choosing sensors that are stable for operating conditions, by implementing interference suppression measures and by measuring gas film stiffness. Finally, the theoretical result is compared to the experimental data to judge the influence of spiral groove structural parameters on gas film stiffness.

2. Analytical model

The structure of the spiral groove gas seal is illustrated in Figure 1. The rotation ring with a micrometer-scale spiral groove on the surface and the shaft sleeve are stabled with the shaft. Meanwhile, the static parts including static ring, springs and spring seats are regarded as the complemental part. The stator ring is made of graphite and the rotor ring is made of SiC. Here, α is the complementary angle of the spiral angle, β is the spiral angle, R_i is the inner radius, R_o is the outer radius, R_r is the root radius, p_i is the inlet pressure and p_0 is the outlet pressure. The seal gas is bubbled into the seal chamber and pumped into the groove from the outer diameter to the groove root. The gas in the groove is compressed

Figure 1 Schematic drawing of the spiral groove dry gas seal

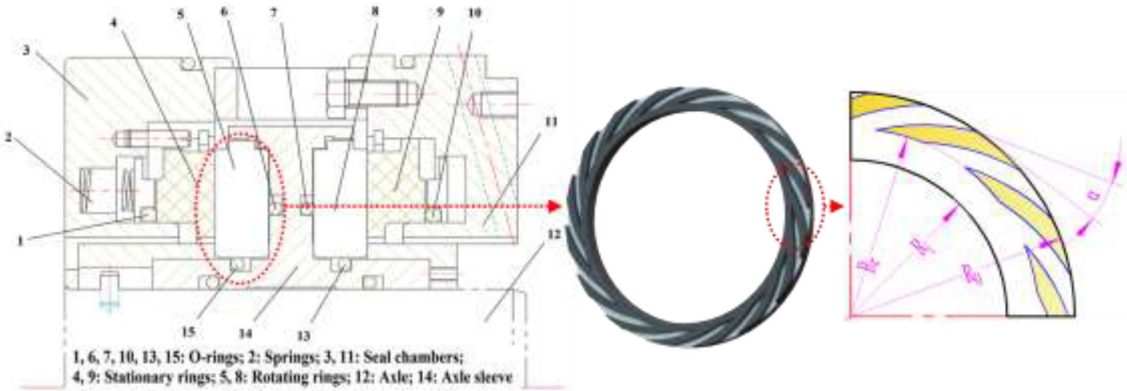

thus, the pressure increases. The seal faces are separated because of the gas film pressure. A layer of thin gas film (about 3–6 μm) is generated between the seal faces.

Reynolds equation under sliding the boundary condition is obtained. And then the approximate analytical equation of gas film opening force is derived. The gas film stiffness is the derivative of the gas film opening force with respect to the gas film thickness.

2.1 Slipping boundary problem

The structure of the spiral groove gas seal is illustrated in Figure 1. The basic assumptions in this work are given as follow:

- The temperature of the sealing gas is steady.
- Gravity and magnetism are ignored.
- The fluid has no slip at the solid interface.
- The gas flow is considered as laminar flow and the gas is a Newtonian fluid.

The General Formula of Navier-Stokes (N-S) equation is as follow:

$$\rho\frac{dv}{dt}=\rho F-\nabla p+\mu\nabla^2 v+\frac{1}{3}\mu\nabla(\nabla\cdot v) \tag{1}$$

The simplified N-S equation in the Cartesian coordinate system can be obtained from the dynamic model of gas flow between two plates:

$$\begin{cases}\dfrac{\partial p}{\partial x}=\dfrac{\partial}{\partial z}\left(\mu\dfrac{\partial u'}{\partial z}\right)\\[2ex]\dfrac{\partial p}{\partial y}=\dfrac{\partial}{\partial z}\left(\mu\dfrac{\partial v'}{\partial z}\right)\end{cases} \tag{2}$$

When the second-order slipping boundary conditions are considered:

$$\begin{aligned}\Big\{u'\,|_{z=0}&=u_0+(l')\frac{\partial u}{\partial z}\,|_{z=0}-\frac{1}{2}\left((l')^2\frac{\partial^2 u}{\partial z^2}\,|_{z=0}u'\,|_{z=h}\right.\\&=-(l')\frac{\partial u}{\partial z}\,|_{z=h}-\frac{1}{2}\left((l')^2\frac{\partial^2 u}{\partial z^2}\,|_{z=h}\right.\end{aligned} \tag{3}$$

$$\begin{aligned}\Big\{v'\,|_{z=0}&=(l')\frac{\partial v}{\partial z}\,|_{z=0}-\frac{1}{2}\left((l')^2\frac{\partial^2 v}{\partial z^2}\,|_{z=0}v'\,|_{z=h}\right.\\&=-(l')\frac{\partial v}{\partial z}\,|_{z=h}-\frac{1}{2}\left((l')^2\frac{\partial^2 v}{\partial z^2}\,|_{z=h}\right.\end{aligned} \tag{4}$$

where:

$$l'=(2-s_v)l/s_v,\ U_o=2\pi n_r R_i,\ h=d(\delta+E)$$

2.2 Micro-scale effect Reynolds equation

Expressions for the circumferential and radial slipping velocities of gas film are written as:

$$u'=\frac{1}{2\eta}\frac{\partial p}{\partial x}(z^2-hz-h\lambda-\lambda^2)+u\left(1-\frac{\lambda+z}{h+2\lambda}\right) \tag{5}$$

$$v'=\frac{1}{2\eta}\frac{\partial p}{\partial y}(z^2-hz-h\lambda-\lambda^2) \tag{6}$$

Using the continuity equation of fluid mechanics:

$$\frac{\partial p}{\partial t}+\frac{\partial}{\partial x}(\rho u')+\frac{\partial}{\partial y}(\rho v')=0 \tag{7}$$

Equation (7) is integrated along the z-direction of the lubricating film thickness:

$$\int_0^h\left[\frac{\partial}{\partial x}(\rho u')+\frac{\partial}{\partial y}(\rho v')\right]dz+\frac{\partial}{\partial t}(\rho h)=0 \tag{8}$$

Assuming that the gas film between the sealed rings is an isothermal flow, the ideal gas state equation is:

$$p=\rho RT \tag{9}$$

Equations (5) and (6) is substituted into equation (8), combining with equation (9), thus the two-dimensional Reynolds equation considering second-order slipping boundary conditions can be written as follow:

$$\frac{\partial}{\partial x}\left[\frac{ph^3}{\mu}\left(1+6\mathrm{Kn}+\frac{2}{3}\mathrm{Kn}^2\right)\frac{\partial p}{\partial x}\right]+\frac{\partial}{\partial y}\left[\frac{ph^3}{\mu}\left(1+6\mathrm{Kn}+\frac{2}{3}\mathrm{Kn}^2\right)\frac{\partial p}{\partial y}\right]=6U_0\frac{\partial(\rho h)}{\partial x} \tag{10}$$

where $\mathrm{Kn}=l\prime/h, h=E+\delta$.

Equation (6) is computed with the non-dimensional method:

$$\frac{\partial}{\partial\phi}\left[PH^3\frac{\partial P}{\partial\phi}\right]+\frac{\partial}{\partial\zeta}\left[PH^3\frac{\partial P}{\partial\zeta}\right]=\chi'\frac{\partial(PH)}{\partial\phi} \tag{11}$$

where,

$$\Lambda=\frac{12\ \pi\mu n_r}{p_i}\frac{R_i^2}{(\delta+E)^2},\chi'=\frac{\Lambda}{\left(1+6\mathrm{Kn}+\frac{2}{3}\mathrm{Kn}^2\right)},\phi=\frac{x}{R_i},\zeta=\frac{y}{R_i}$$

The boundary conditions in the dimensionless form are:

$$\begin{cases}P_{(\zeta=1)}=1\\ P_{(\zeta_0=R_0/R_i)}=p_o/p_i\end{cases} \tag{12}$$

2.3 Approximate analytical formula of gas film opening force and stiffness

The PH linear method is used in combination with the iteration method to solve equation (11). And then it can be integrated from the inner radius to the outer radius in a rotating ring. The equation of gas film opening force is as follows:

$$F=2\ \pi\int_{R_i}^{R_o}rp\mathrm{d}r$$

$$=\left[\frac{p_i}{1-\varepsilon_z\cos\varphi-\frac{E\cos\omega}{E+\delta}}+\frac{\frac{Ep_i}{E+\delta}\left(\eta_{1(\zeta)}\cos\omega+\eta_{2(\zeta)}\cos\omega\right)}{1-\varepsilon_z\cos\varphi-\frac{E\cos\omega}{E+\delta}}\right.$$

$$\left.-\frac{3}{2}\beta_0\left(\frac{E}{E+\delta}\right)^2\eta_{2(\zeta)}(\zeta_0-\zeta)p_i\right]\left(\pi R_o^2-\pi R_i^2\right) \tag{13}$$

where,

$$\eta_{1(\zeta)}=c_{10}e^{\sqrt{\beta_1}\zeta}+c_{10}'e^{-\sqrt{\beta_1}\zeta}+\left(c_{11}e^{\sqrt{\beta_1}\zeta}+c_{11}'e^{-\sqrt{\beta_1}\zeta}+\frac{A_1}{2\sqrt{\beta_1}}\zeta e^{\sqrt{\beta_1}\zeta}-\frac{B_1}{2\sqrt{\beta_1}}\zeta e^{-\sqrt{\beta_1}\zeta}\right)\varepsilon,$$

$$\eta_{2(\zeta)}=c_{20}e^{\sqrt{\beta_1}\zeta}+c_{20}'e^{-\sqrt{\beta_1}\zeta}+\left(c_{21}e^{\sqrt{\beta_1}\zeta}+c_{21}'e^{-\sqrt{\beta_1}\zeta}+\frac{A_2}{2\sqrt{\beta_1}}\zeta e^{\sqrt{\beta_1}\zeta}-\frac{B_2}{2\sqrt{\beta_1}}\zeta e^{-\sqrt{\beta_1}\zeta}-\frac{\alpha_2}{\beta_1}\right)\varepsilon,$$

$$\beta_1=\beta_0^2+n^2,h=H(E+\delta),\beta_0=n\tan\alpha,\omega=n\varphi+\beta_0\zeta$$

The gas film stiffness is called as the axial stiffness of gas film in dry gas seal. Thus, the gas film stiffness is the derivative of the gas film opening force with respect to the gas film thickness and can be presented as:

$$K_g=\frac{\mathrm{d}F}{\mathrm{d}\delta}=\frac{Ep_i(\ \pi R_o{}^2-\ \pi R_i{}^2)}{(\delta+E)^2\left(1-\varepsilon_z\cos\varphi-\frac{E\cos\omega}{\delta+E}\right)^2}$$

$$\times\left(\left(\eta_{1(\zeta)}\cos\omega\cos\varphi\varepsilon_z+\eta_{2(\zeta)}\sin\omega\cos\omega\varepsilon_z\right)\right.$$

$$\left.-\left(\eta_{1(\zeta)}\cos\omega+\eta_{2(\zeta)}\sin\omega+\cos\omega\right)\right)+3\left(\ \pi R_o{}^2-\ \pi R_i{}^2\right)p_i$$

$$\beta_0\eta_{2(\zeta)}(\zeta_0-\zeta)E^{2(\delta+E)-3} \tag{14}$$

3. Experiments

3.1 Test bench system

A test bench with a spiral groove dry gas seal is used in the test experiments. This bench includes four major components, namely, a seal, gas path and testing system, as illustrated in Figure 2. The gas pressure is 0–5 MPa and the rotational speed can be adjusted freely in the range of 100–5,000 r/min. The seal system that serves as the research object in this study is a spiral groove dry gas seal with a series structure. The test system consists of hardware devices (sensor, data acquisition units, etc.) and software (LabVIEW).

3.2 Selection and placement of sensor

The general displacement sensor is difficult to make an accurate response to the micron gap of the seal face with extremely thin film thickness and minimal vibration displacement. On the other hand, the tested parts must have good electrical conductivity and a smooth surface, so it is

Figure 2 Schematic drawing of test bench (a) and the structures of gas, testing and sealing systems (b)

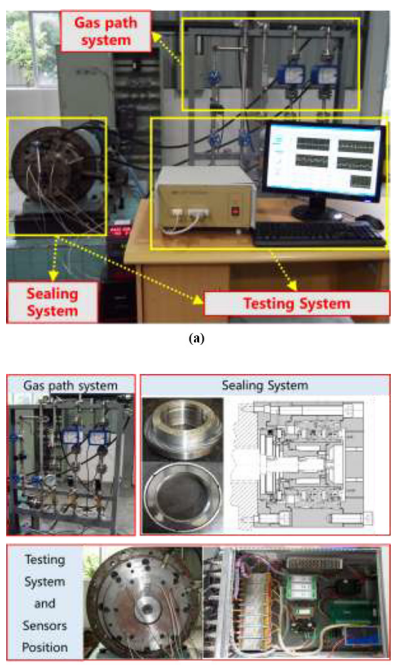

exceedingly difficult to measure. In this experiment, the high precision improved microsensor is selected, the tungsten carbide is selected as the material of the rotating ring and graphite is selected as the material of the static ring.

A modified eddy current sensor Model ST-GL is implemented to measure the thickness of the gas film between the rings in the experiment. Eddy current sensors based on high frequency eddy current effect are a kind of non-contact sensor to measure the displacement and the vibration. Three sensors are placed 120° from one to another circumferentially at the same radial position in the static ring (Figure 3). The probes should be rubbed with the static ring to parallel the probes and the static ring face.

The test of the vibrative displacement of static ring: a modified displacement eddy current sensor Model ST-2 is selected. The sensors are fixed in the inner of the end cap. The sensors' probes are flushed against the back side of the stationary ring face. Three sensors are installed 120° in circumferential and 112 mm in the radial distance (Figure 3).

3.3 Test principles of gas film stiffness

The schematic diagram of the seal test structure is shown in Figure 4. In this experiment, for the construction of the dry gas seal test bench, sensors are installed in the corresponding parts of the sealing system to collect the physical signals of the vibration displacement of the gas film and the static ring, combined with the corresponding hardware equipment such as the preprocessor, the signal conditioning module, the data acquisition card and the output terminal.

The testing data of gas film: first, a fixed length is chosen for data of the gas film to reduce computing time. Second, the median filter is applied to process the data. The displacement curve of the gas film is obtained after smooth-going. Third, the method of Fast Fourier Transform (FFT) is key to handle with the displacement curve, which is translated into the spectrum curve of gas film vibration. And then, the testing data of the stationary ring need to be processed as well. The handling method of the static ring is similar with the data of gas film. The testing data of the stationary ring: the fixed length of data is chosen and the median filter is applied as well and then the spectrum curve of stationary ring vibration is plotted by FFT.

Figure 3 Sensors of gas film and stationary ring vibration are placed

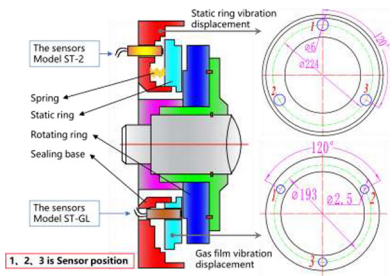

Figure 4 The schematic diagram of the seal test structure

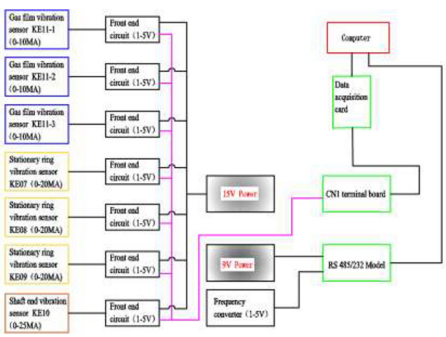

The gas film stiffness $K_g^{'}$ can be obtained by face opening force F_o and gas film thickness δ tested. For dry gas seal, the opening force F_o must be equal to the closing force F_c during steady state:

$$F_o = F_c \tag{15}$$

where

$$F_c = p_i A_e + K_s \Delta x \tag{16}$$

According to the operation of dry gas seal, the spring displacement value is equal to stationary ring axial displacement value. Thus, the variable value of gas film opening force is equal to the variable value of spring force. The gas film stiffness for test technology can be written as follow:

$$K_g^{'} = \Delta F / \Delta \delta = K_s \Delta x / \Delta \delta \tag{17}$$

where $\Delta\delta$ is the variable value gas film displacement (gas film axial vibration value), K_s is the spring stiffness, Δx is the variation value of stationary ring displacement (stationary ring axial vibration value).

3.4 Spiral groove engraving

A pulsed solid-state yttrium aluminium garnet laser with a pulse width in the range of 30 fs to 30 ps is used. The engraving process is as follows:

- The laser power is set to 80%, and the engraving is performed repeatedly at this power to obtain the required depth of the texture.
- The laser power is set to 50%. The surface is scanned, and finishing is performed on the texture areas that meet the depth requirement. The uneven bottoms of the texture areas are repaired, and the roughness is improved.
- The laser power is reduced to 20%. The burr on the edge of the pattern has been improved.

The spiral groove surface profile of the rotating ring is scanned, and a white-light interference three-dimensional profiler is used, as shown in Figure 5.

3.5 Anti-jamming measurement

The interference of electromagnetic energy must affect the sensitive sensors. According to the above cases, we have the following several anti-jamming measures:

- The use of grounding technology suppresses the interference.
- The length of the conducting wire is minimized, and the high-density shielding copper grid is used.

Figure 5 Morphology of spiral groove

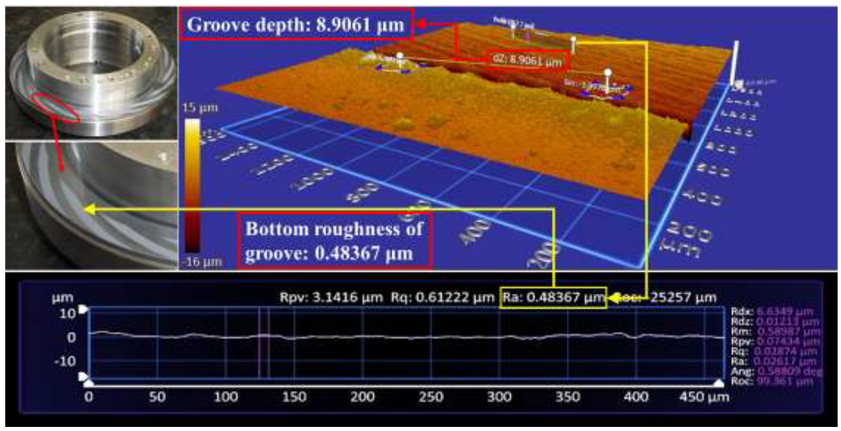

- The test bench, test instrument and computer are placed closely to improve the anti-interference performance of the transmission channel.
- A high-input impedance collecting card (the input impedance is increased from 10 M to 1 G) is customized to ensure that the interference current has no effect on the incoming signal.
- The collecting card adopts two-side input (the positive and negative channel input one-channel signal) so that the common-mode interfering signal can be effectively reduced, and the anti-interference performance of the test equipment can be improved.

3.6 Test procedure

The experiment is divided into five groups, the rotational speed range is 2,000–4,000 r/min and the rotational speed of each group increased by 500 r/min. At the same time, the pressure is tested five times at each group and the pressure range of 1.0–3.0 r/min is increased by 0.5 MPa each time, as shown in Table 1. According to the theoretical calculation results, the optimized spiral groove parameters are obtained and two types of rotating rings are processed, which are the normal spiral groove rotating ring and the optimized spiral groove rotating ring, respectively. Under the condition of keeping the structure of the seal prototype unchanged, the rotating ring is replaced. The specific process is as follows:

First, install the sealing prototype of the normal spiral groove on the test bench and connect the test system with the gas path system.

Second, the gas pressure 0.5 MPa is pump into the sealing system and judge the torque. If the torque is small, the motor can be started.

Third, the motor is started from 1,000 r/min to warm up the machine for 30 min, then carry out the experimental operation and record the experimental data according to Table 1.

Fourth, when the experiment finishes, the motor is turn off and then gradually reduces the gas pressure to 0.1 MPa.

Fifth, the seal prototype is dismantled and then replace the normal spiral groove rotating ring with the optimized spiral groove rotating ring and repeat the (2)–(4) steps to carry out the experiment.

4. Results and discussion

Table 2 shows the structure, physical and operation parameters. The gas film stiffness for spiral groove dry gas seal is studied by theoretical calculation.

4.1 Influence of medium pressure and rotating speed

In this analysis, the medium pressure and gas film thickness are varied, while the remaining factors are unchanged. The result from this analysis is shown in Figure 6(a). That is, as the medium pressure increase, the trend of the gas film stiffness ascends. The value of gas film stiffness is from 2×10^7 N/m to 8.2×10^7 N/m. The gas film stiffness increases by approximately 2×10^7 N/m from 1 to 1.5 MPa, 1.7×10^7 N/m from 1.5 to 2 MPa, 1.2×10^7 N/m from 2 to 2.5 MPa and 1.3×10^7 N/m from 2.5 to 3 MPa. Figure 6(a) also shows the gas film stiffness continuously decreases with an increase in gas film thickness. It can be observed that the gas film stiffness presents nonlinearity because of gas compressibility. According to equation (16), the medium pressure affects value of the closing force. When the medium pressure becomes large, the closing force would to be increased. However, the opening

Table 1 The experimental operation condition and order

No.	Rotating speed/(r/min)	Sealing pressure (medium pressure)/MPa					Time/s
		p_1	p_2	p_3	p_4	p_5	
1	2,000	1.0	1.5	2.0	2.5	3.0	1,500
2	2,500	1.0	1.5	2.0	2.5	3.0	1,500
3	3,000	1.0	1.5	2.0	2.5	3.0	1,500
4	3,500	1.0	1.5	2.0	2.5	3.0	1,500
5	4,000	1.0	1.5	2.0	2.5	3.0	1,500

Table 2 The structure, physical and operation parameters of the seal rings

Parameter	Name	Value	Parameter	Name	Value
R_i	Inner radius	0.086 m	α	Complementary angle of spiral angle	0.279 rad
R_o	Outer radius	0.114 m	β	Spiral angle	1.292 rad
R_r	Root radius	0.102 m	$2E$	Groove depth	0.8×10^5 m
R_e	Slip radius	0.0945 m	n	Number of spiral grooves	16
A_e	Effective area of the stationary ring	0.013 m^2	K_s	Spring stiffness	15.4 N/mm
L	Axial length of stationary ring	0.014 m	n_s	Number of springs	12
μ	Dynamic viscosity of gas	1.8247×10^{-5}Pa · s	ρ	Gas density	1.1885kg/m^3
σ_v	Coefficient of the molecular tangential momentum	1	l	Molecular free path	6.89×10^{-8}m

Figure 6 Curve surface of gas film stiffness under (a) medium pressures and (b) rotating speed

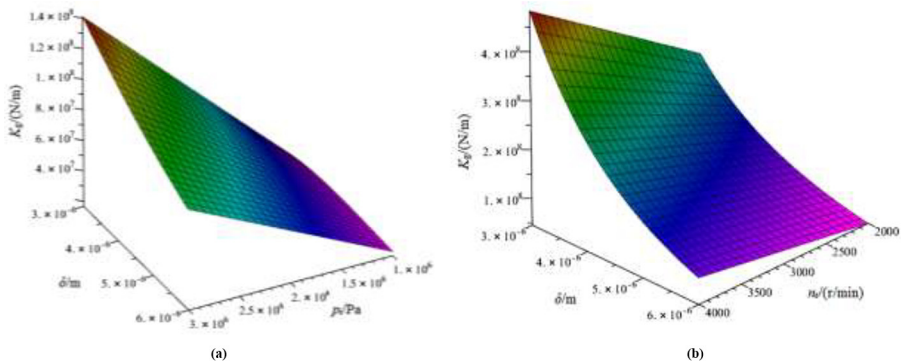

force must be equal to the closing force. Thus, the film thickness needs to be decreased. Finally, the variation in film thickness would make the gas film stiffness increase. It can be observed that the gas film stiffness presents nonlinearity because of gas compressibility.

In this analysis, the varied factors are rotating speed and gas film thickness. The result from this analysis is plotted in Figure 6(b). According to the below figure, it can be observed that as the rotating speed increases, the trend of the gas film stiffness ascends. The value of gas film stiffness is from 5.5×10^7 N/m to 1.0×10^8 N/m. The gas film stiffness increases by approximately 1.6×10^7 N/m from 2,000 to 2,500 r/min, 1.1×10^7 N/m from 2,500 to 3,000 r/min, 0.8×10^7 N/m from 3,000 to 3,500 r/min and 1.0×10^7 N/m from 3,500 to 4,000 r/min. Figure 6(b) also shows the gas film stiffness value continuously decreases with an increase in gas film thickness. The results from this analysis show a similar trend to Figure 6(a) in direction of film thickness. The gas film pressure comes from the hydrodynamic effect of the spiral groove, meanwhile, the hydrodynamic effect is directly proportional to the rotational speed. Thus, the increase of rotating speed causes an increase in the gas film pressure. Finally, the gas film stiffness becomes larger.

A comparison of Figures 6(a) and 6(b) clearly shows the following: the variation trend of gas film stiffness at medium pressures is similar to that at rotating speeds. The influence of rotating speed on gas film stiffness is greater than that of medium pressure. The results demonstrate that relatively small the gas film thickness can achieve higher gas film stiffness. It also can be inferred that increasing medium pressure and rotating speed can achieve higher gas film stiffness. It is confirmed that the gas film stiffness with relatively small gas film thickness, high medium pressure and high rotating speed can improve the dynamic characteristic of dry gas seal. Thus, dry gas seal is steadier at high operation conditions.

4.2 Influence of spiral angle and groove depth

The theoretical model can optimize gas film stiffness of a spiral groove dry gas seal under a specific operation condition, which makes dry gas seal system high stiffness and stability in running process. In this section, how the structural parameters of spiral groove dry gas seal improve the gas film stiffness is discussed.

Figure 7(a) depicts the effect of spiral angle and gas film thickness on the gas film stiffness under the condition of rotational speed 4,000 r/min and pressure 3 MPa. The situation of gas film stiffness with spiral angle is as follows: the value of gas film stiffness first increases and then deceases with an increase in spiral angle. For the spiral angle, when spiral angle is high ($\beta > 1.32$ rad) in Figure 7(a), the spiral groove dry gas seal can obtain higher gas film stiffness. However, the fluctuation in gas film stiffness is smaller during 1.22–1.32 rad. Thus, an optimal spiral angle is clearly seen for maximum gas film stiffness. The new spiral angle is 1.34 rad (76.8°), the gas film thickness is 3.0×10^{-6} m and the new gas film stiffness is 1.6×10^8 N/m.

Figure 7(b) presents the gas film stiffness as a function of the gas film thickness and groove depth (E is half of the groove depth and $2E$ is groove depth) under the condition of rotational speed

Figure 7 Curve surface of gas film stiffness under (a) spiral angle and (b) groove depth

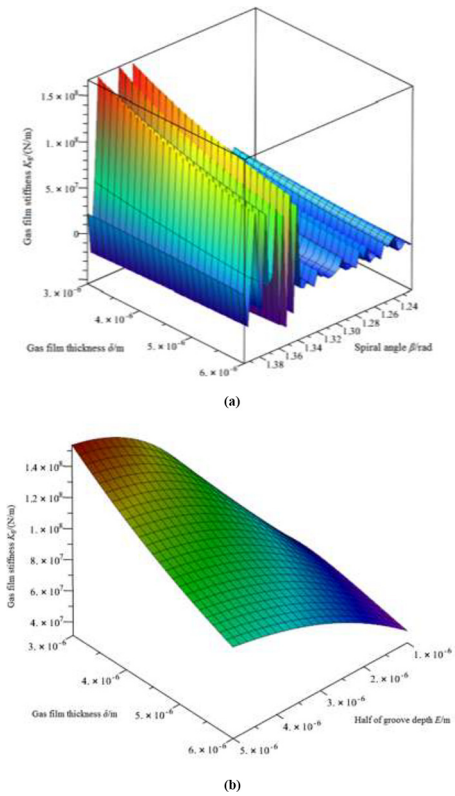

4,000 r/min and pressure 3 MPa. It can be found that the gas film stiffness increases as groove depth increases, whereas the gas film stiffness decreases as the gas film thickness increases. The situation of gas film stiffness changes with groove depth is explained as follows: when the groove depth of rotating ring surface deepens gradually, the rates of inhaling and compressed gas of spiral groove accelerate. Thus, the gas film stiffness is larger. When $E < 4 \times 10^{-6}$ m, the effect of groove depth on the gas film stiffness is significant. However, when $E > 4 \times 10^{-6}$ m, it can be seen the gas film stiffness does not change drastically and goes to a maximum value about 1.8×10^{8} N/m. Thus, an optimal groove depth is clearly seen for maximum gas film stiffness. The new groove depth is 1×10^{-5} m (E is 5×10^{-6} m, $2E$ is 1×10^{-5} m), the gas film thickness is 3.0×10^{-6} m and the new gas film stiffness is 1.8×10^{8} N/m.

Comparison of Figures 7(a) and 7(b) provides the following results:

An optimum value of the spiral angle and half of the groove depth for maximum gas film stiffness is clearly seen. The gas film stiffness can be improved effectively after the structural parameters of the spiral groove are optimized. Moreover, by comparing Figures 7(a) and 7(b), it can be demonstrated that the effect of spiral angle on the gas film stiffness is larger than half of the groove depth. When the gas film thickness is 3.0×10^{-6} m, the optimized groove depth and spiral angle is 1×10^{-5} m and 76.8°, respectively.

4.3 Test verification of gas film stiffness

The gas film stiffness for the spiral groove dry gas seal is studied by theoretical calculation. The gas film stiffness can be improved effectively after the structural parameters of the spiral groove are optimized. An optimum value of the spiral angle and groove depth for improved gas film stiffness is clearly seen. The optimization range of the structural parameters of the spiral groove to improve gas film stiffness is as follows: spiral angle is 1.34 rad (76.8°) and groove depth is 1×10^{-5} m. And then, the normal and optimized rotating rings of the spiral groove are processed and carved. Thus, the dry gas seal optimized is run and tested in the test bench. In the following sub-structural content, the experimental results are compared with the above theoretical results. Table 3 list the structure parameters of the spiral groove for the normal and optimized rotating rings. The dry gas seal optimized is run and tested in the test bench.

4.3.1 Gas film thickness under medium pressure and rotating speed

Figure 8 is the gas film thickness obtained from the test under the condition of rotational speed 4,000 r/min and medium pressure 3 MPa. Figure 8(a) shows that the experimental gas film thickness of medium pressure 3 MPa is based on the speed of 4,000 r/min and Figure 8(b) is that the experimental gas film thickness of speed 4,000 r/min is based on the medium pressure 3 MPa. It can be seen from Figure 8 that the experimental gas film thickness obtained by constant speed and variable pressure is slightly different from that obtained by constant pressure and variable speed. The experimental gas film thickness of Figure 8(a) is 2.6×10^{-6} m and that of Figure 8(b) is 2.7×10^{-6} m. Therefore, under the condition of rotational speed 4,000 r/min and medium pressure 3 MPa, the experimental average gas film thickness is 2.65×10^{-6} m under the condition of rotational speed 4,000 r/min and pressure 3 MPa; meanwhile, the theoretical gas film thickness is 3.0×10^{-6} m. The error between the experimental gas film thickness and the theoretical gas film thickness is only 13.21%, which proves that the theoretical gas film thickness is consistent with the experimental gas film thickness.

4.3.2 Gas film stiffness under medium pressure and rotating speed.

The experimental data are substituted into equation (17). Then, gas film stiffness is plotted against medium pressure in Figure 9(a). Figure 9(a) shows that the experimental gas film stiffness value continuously increases with an increase in pressure. The value of experimental gas film stiffness is from 6×10^{7} N/m to 1.16×10^{8} N/m. The gas film stiffness increases by approximately 2.1×10^{7} N/m from 1 to 1.5 MPa, 0.3×10^{7} N/m from 1.5 to 2 MPa, 1.2×10^{7} N/m from 2 to 2.5 MPa and 2×10^{7} N/m from 2.5 to 3 MPa. Meanwhile, the theoretical gas film stiffness value has a same trend in Figure 9(a). The experimental gas film stiffness of the optimized spiral groove is always higher than that of the normal spiral groove. Meanwhile, the trend of the theoretical optimized value is consistent with the experimental results. What is more, the theoretically optimized gas film stiffness is closer to the experimental gas film stiffness of the optimized spiral groove. It is confirmed that the structural parameter of spiral groove optimized enhancing gas film stiffness of dry gas seal.

The experimental data are substituted into equation (17). Then, gas film stiffness is plotted against rotating speed in Figure 9(b). It can be found that as the rotating speed increases, the trend both of the experimental and theoretical gas film ascends. The experimental value of gas film stiffness is from 1.12×10^{8} N/m to 1.47×10^{8} N/m. The gas film stiffness increases by approximately 0.3×10^{7} N/m from 2,000 to 2,500 r/min, 0.1×10^{7} N/m from 2,500 to 3,000 r/min, 1.9×10^{7} N/m from 2,000 to 3,500 r/min and 1.2×10^{7} N/m from 3,500 to 4,000 r/min. Meanwhile, when

Table 3 The structure parameters of spiral groove for the normal and optimized rotating rings

Parameter	Name	Value	Parameter	Name	Value
The normal rotating ring of spiral groove			*The optimized rotating ring of spiral groove*		
β	Spiral angle	1.292 rad	β	Spiral angle	1.34 rad
$2E$	Groove depth	0.8×10^5 m	$2E$	Groove depth	1×10^5 m
n	Number of spiral grooves	16	n	Number of spiral grooves	16

Figure 8 The experimental gas film thickness under (a) medium pressure 3 MPa and (b) speed 4,000 r/min

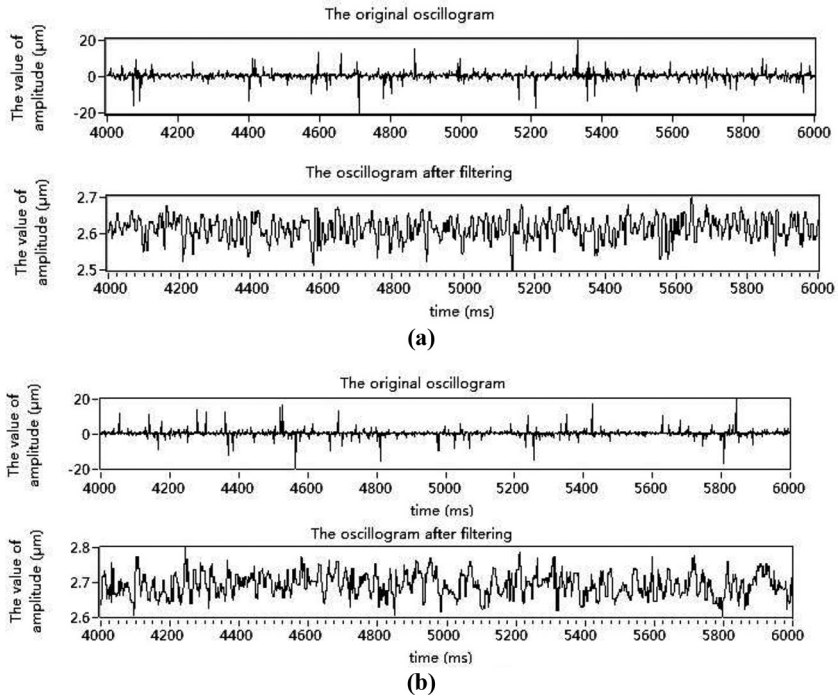

Figure 9 Curve of the theoretical and experimental gas film stiffness under (a) medium pressure and (b) rotating speed

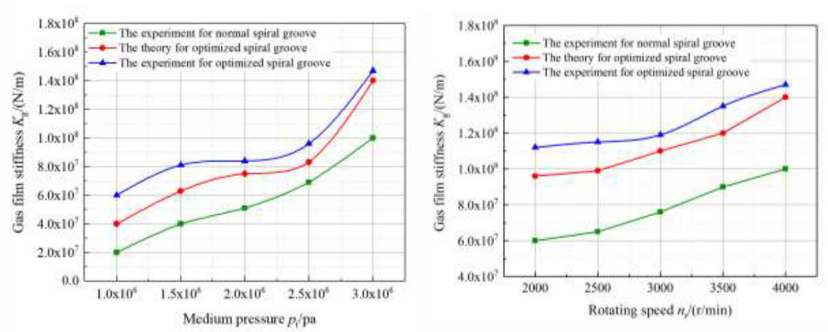

rotating speed is low (n_r < 3,000 r/min) in Figure 9(b), experimental value does not change drastically. However, for n_r > 3,000 r/min, it can be seen the effect of rotating speed on the gas film stiffness is significant. The result shows that rotating speed is higher, the gas film stiffness changes more quickly. The experimental gas film stiffness of the optimized spiral groove is always higher than that of the normal spiral groove. Meanwhile, the trend of the theoretical optimized value is consistent with the experimental results, but the theoretically optimized gas film stiffness is closer to the experimental value of the optimized spiral groove visibly. It is also shown that structural parameters of spiral groove optimized enhancing gas film stiffness of dry gas seal. The optimization of gas film stiffness can be guided by theoretical calculation.

Table 4 Comparative data of theoretical and experimental gas film stiffness

Operation		The theoretical value for optimized spiral groove	The experimental value for optimized spiral groove	Error (%)
Pressure	1.0 × 10^6 Pa	4.0 × 10^7 N/m	6.0 × 10^7 N/m	33.33
	1.5 × 10^6 Pa	6.3 × 10^7 N/m	8.1 × 10^7 N/m	22.22
	2.0 × 10^6 Pa	7.5 × 10^7 N/m	8.4 × 10^7 N/m	10.71
	2.5 × 10^6 Pa	8.3 × 10^7 N/m	9.6 × 10^7 N/m	13.54
	3.0 × 10^6 Pa	1.4 × 10^8 N/m	1.47 × 10^8 N/m	4.76
Speed	2,000 r/min	9.6 × 10^7 N/m	1.12 × 10^8 N/m	14.29
	2,500 r/min	9.9 × 10^7 N/m	1.15 × 10^8 N/m	13.91
	3,000 r/min	1.1 × 10^8 N/m	1.19 × 10^8 N/m	7.56
	3,500 r/min	1.2 × 10^8 N/m	1.35 × 10^8 N/m	11.11
	4,000 r/min	1.4 × 10^8 N/m	1.47 × 10^8 N/m	4.76

4.3.3 Error analysis

Table 4 shows the comparative data of theoretical gas film stiffness and experimental gas film stiffness with spiral groove optimization. The following points can be found:

- In the process of pressure adjustment: the maximum error is 33.33%, which appears in the position where the pressure is 1 MPa; the minimum error is 10.71%, which appears in the position where the pressure is 2 MPa.
- In terms of rotational speed: the maximum error is 14.29%, which appears at 2,000 r/min and the minimum error is 4.76%, which appears at 4,000 r/min.
- The average error is less than 20%.

Therefore, the validity of the theoretical model is verified. However, there is still a certain gap between the theory and the test and the maximum error basically appears in the low speed and low-pressure stage. The reasons for the error are as follows:

- The dry gas seal is unstable at low speed and low pressure, which leads to interference in the test.
- Because the gas film gap is too small to arrange more sensors in a smaller area, it is impossible to fully measure the operation of the whole gas film and static ring.
- The sensor is installed by landfill method, but it cannot accurately guarantee that the probe of the sensor is completely flush with the surface of the static ring, which interferes with gas flow in the micro-gap.
- Installation error and deformation are not considered in the theoretical calculation.

5. Conclusion

The gas film stiffness of a spiral groove dry gas seal based on a theoretical calculation, parameter optimization and test technology are investigated. Based on the above results, we draw the following conclusions:

- A theoretical procedure based on the asymptotic methods for the compressible Reynolds equation for seal faces and gas film is implemented to research the gas film stiffness under different operation conditions. The value of gas film stiffness increases with an increase in medium pressure and rotational speed.
- The relationship between the structural parameters of the spiral groove dry gas seal and the gas film stiffness is identified and optimized. The optimization rang of the structural parameters of the spiral groove is obtained.
- The dry gas seal optimized is tested in the test bench. Comparison of theoretical and experimental results, the test and theoretical value of gas film stiffness has a same trend. However, a higher gas film stiffness is appeared after optimizing the structural parameters. It proves that an increase of gas film stiffness can be guided by theoretical calculation.

In conclusion, dry gas seal is steadier at high operation conditions. The new gas film stiffness is improved after optimizing the structural parameter. The study reveals some of the characteristics of gas film stiffness of dry gas seals, which may help improve seal performance and extend seal lifetime.

Acknowledgement

The work presented is supported by the National Natural Science Foundation of China under Award No. 51905480, the Ningbo science and technology innovation 2025 major projects, China, under Award No. 2020Z112 and the National Natural Science Foundation of Ningbo, China, under Award No. 2019A610161.

Research interests: Mechanical friction, wear and lubricationIn terms of scientific research, he has successively presided over the National Natural Science Foundation, and Ningbo Natural Science Foundation, China. Meanwhile, he participated in many scientific research projects such as the "Science and Technology Innovation 2025" project. A total of more than 10 papers have been published in the past five years, including 3 in SCI, 6 in EI, 1 in SCI-TOP journals and 1 in ESI.

References

Bai, S.X., Huang, P., Meng, Y.G. and Wen, S.Z. (2006), "Modeling and analysis of interfacial electro-kinetic effects on thin film lubrication", *Tribology International*, Vol. 39 No. 11, pp. 1405-1412.

Ding, X.X. and Lu, J.J. (2016), "Theoretical analysis and experiment on gas film temperature in a spiral groove dry gas seal under high speed and pressure", *International Journal of Heat and Mass Transfer*, Vol. 96, pp. 438-450.

Ding, X.X., Zhang, Y.J., Liu, B. and Liu, Y. (2014), "Calculation and analysis of gas film stiffness in the spiral

groove gas seal under the thermal dissipation", *Chinese Journal of Applied Mechanics*, Vol. 31 No. 6, pp. 859-864.

Du, W.Q. and Zhang, D. (2019), "Research on the performance of supercritical CO2 dry gas seal with different deep spiral groove", *Journal of Thermal Science*, Vol. 28 No. 3, pp. 547-558.

Huang, W.F., Lin, Y.B., Gao, Z., Fan, W.J., Suo, S.F. and Wang, Y.M. (2013), "An acoustic emission study on the starting and stopping processes of a dry gas seal for pump", *Tribology Letters*, Vol. 49 No. 2, pp. 379-384.

Huang, W.F., Lin, Y.B., Liu, Y., Liu, X.F., Gao, Z. and Wang, Y. M. (2013), "Face rub-impact monitoring of a dry gas seal using acoustic emission", *Tribology Letters*, Vol. 52 No. 2, pp. 253-259.

Jacobs, W., Boonen, R., Sas, P. and Moens, D. (2014), "The influence of the lubricant film on the stiffness and damping characteristics of a deep groove ball bearing", *Mechanical Systems and Signal Processing*, Vol. 42 Nos 1/2, pp. 335-350.

Jiang, J.B., Peng, X.D., Li, J.Y. and Chen, Y. (2016), "A comparative study on the performance of typical types of bionic groove dry gas seal based on bird wing", *Journal of Bionic Engineering*, Vol. 13 No. 2, pp. 324-334.

Jin, Z.X., Li, S.X., Cai, J.N. and Zhang, Q.X. (2016), "Optimizing on hydrostatic structural parameters for regulatable dry gas seal based on central composite design test", *Industrial Lubrication and Tribology*, Vol. 68 No. 1, pp. 99-105.

Kollinger, R. (1989), "Theoretical and experimental investigation into the running characteristics of gas-lubricated mechanical seals". *12th International Conference on Fluid Scaling*, Brighton, pp. 307-322.

Kolomoets, A. and Dotsenko, V. (2012), "Experimental investigation of dry gas-dynamic seals used for gas-compressor unit", *Procedia Engineering*, Vol. 39, pp. 379-386.

Kou, G., Li, X., Wang, Y., Lin, M., Tan, C. and Mou, M. (2020), "Steady performance and dynamic characteristics of a superellipse groove dry gas seal at a high-speed condition", *Industrial Lubrication and Tribology*, Vol. 72 No. 6, pp. 789-796.

Liu, R., Wang, X.L. and Zhang, X.Q. (2012), "Effects of gas rarefaction on dynamic characteristics of micro spiral-grooved thrust bearing", *Journal of Tribology*, Vol. 134 No. 2, pp. 022201-022207.

Lu, J.J. (2020), "Theoretical optimization and experiment on lubrication of floating microgroove cylindrical seal", *Industrial Lubrication and Tribology*, Vol. 72 No. 10, pp. 1217-1226.

Lu, J.J., Wang, T.R., Ding, X.X., Song, H. and Li, H. (2021), "Tribological performance of friction pairs with different materials and bi-composite surface texture configurations", *Applied Sciences*, Vol. 11 No. 11, pp. 4738-4757.

Miller, B.A. and Green, I. (2002), "Numerical techniques for computing rotordynamic properties of mechanical gas face seals", *Journal of Tribology*, Vol. 124 No. 4, pp. 755-761.

Miller, B.A. and Green, I. (2003), "Semi-analytical dynamic analysis of spiral grooved mechanical gas face seals", *Journal of Tribology*, Vol. 125 No. 2, pp. 403-413.

Nagai, K., Kaneko, S., Taura, H. and Watanabe, Y. (2018), "Numerical and experimental analyses of static characteristics for liquid annular seals with helical grooves in seal stator", *Journal of Tribology*, Vol. 140 No. 3, pp. 032201-032216.

Sawicki, J.T. and Rao, T. (2004), "A nonlinear model for prediction of dynamic coefficients in a hydrodynamic journal bearing", *International Journal of Rotating Machinery*, Vol. 10 No. 6, pp. 507-513.

Shen, Y.J., Peng, H.B., Li, X.H. and Yang, S.P. (2017), "Analytically optimal parameters of dynamic vibration absorber with negative stiffness", *Mechanical Systems and Signal Processing*, Vol. 85, pp. 193-203.

Shi, L.P., Wang, X.Y., Su, X., Huang, W. and Wang, X. (2016), "Comparison of the load-carrying performance of mechanical gas seals textured with microgrooves and microdimples", *Journal of Tribology*, Vol. 138 No. 2, pp. 021701-021707.

Xu, W.J. and Yang, J.G. (2016), "Spiral-grooved gas face seal for steam turbine shroud tip leakage reduction: performance and feasibility analysis", *Tribology International*, Vol. 98, pp. 242-252.

Yu, P.L., Chen, X.D., Wang, X.L. and Jiang, W. (2015), "Frequency-dependent nonlinear dynamic stiffness of aerostatic bearings subjected to external perturbations", *International Journal of Precision Engineering and Manufacturing*, Vol. 16 No. 8, pp. 1771-1777.

Zhang, X., Jiang, J.B., Peng, X. and Li, J. (2021), "Leakage and rotordynamic characteristics of labyrinth seal and hole-pattern damping seal with special-shaped 3D cavity", *Industrial Lubrication and Tribology*, Vol. 73 No. 2, pp. 396-403.

About the author

Junjie Lu, PhD in Engineering. The leading talent training program of colleges and universities in Zhejiang province-young talents, China. He graduated from Lanzhou University of Technology, China, in June 2018, and then worked in Ningbo Institute of Technology of Zhejiang University, China, in September 2018. Junjie Lu can be contacted at: lovelj4566@163.com